

Dynamics of vortex nucleation by rapid thermal quench

I. S. Aranson,¹ N. B. Kopnin,^{2,3} and V. M. Vinokur¹

¹Argonne National Laboratory, 9700 South Cass Avenue, Argonne, Illinois 60439

²Low Temperature Laboratory, Helsinki University of Technology, P.O. Box 2200, FIN-02015 HUT, Finland

³L. D. Landau Institute for Theoretical Physics, 117334 Moscow, Russia

(Received 7 November 2000; published 29 March 2001)

By numerical and analytical studies of the time-dependent Ginzburg-Landau model we show that vortex nucleation in superfluid ^3He by rapid thermal quench in the presence of superflow is dominated by a transverse instability of the moving normal-superfluid interface. The instability threshold is found analytically as a function of supercurrent density and the front velocity. The dynamics of vortex evolution at long times after the quench is investigated.

DOI: 10.1103/PhysRevB.63.184501

PACS number(s): 74.40.+k, 67.57.Fg, 05.70.Fh

I. INTRODUCTION

Formation of topological defects under a rapid quench is a fundamental problem of contemporary physics promising to shed a new light on the early stages of the evolution of the Universe. For homogeneous cooling a fluctuation-dominated formation mechanism has been suggested by Kibble and Zurek (KZ).¹⁻³ Normally, cooling is associated with an inhomogeneous temperature distribution accompanied by a phase separating interface which moves through the system as temperature decreases. A generalization of the KZ scenario was suggested in Ref. 4 for inhomogeneous phase transitions in superfluids: if the thermal front moves faster than the normal-superfluid interface a large supercooled region which is left behind becomes unstable towards fluctuation-induced nuclei.

Superfluid ^3He offers a unique “testing ground” for rapid phase transitions.⁵ In recent experiments with a rotating superfluid ^3He , vortex formation was revealed during a rapid second-order phase transition triggered by absorption of neutrons.^{6,7} The sample was locally heated well above the critical temperature due to the energy produced by each absorption event. The heated region then cooled down rapidly below the superfluid transition. Such an inhomogeneous cooling is associated with propagation of normal-superfluid (NS) interface and with formation of a large supercooled normal region behind the interface.^{4,8} The fluctuation-dominated mechanism may thus be responsible for creation of initial vortex loops in the supercooled region. It is commonly accepted that these initial vortex loops are further inflated by the superflow and give rise to a macroscopic number of large vortex lines filling the bulk superfluid.

In this paper we report a different mechanism of the vortex formation which overtakes the growth of the initial fluctuation-dominated loops. Preliminary account of some results had been published in Ref. 9. Studying the entire process of the vortex formation in the presence of a superflow using the time-dependent Ginzburg-Landau (TDGL) dynamics, we account for the temperature evolution assuming a thermal diffusion. The TDGL scheme is modified to allow for a complex relaxation rate which models the vortex dynamics at temperatures considerably below T_c .

We find analytically and confirm by numerical simula-

tions that the NS interface becomes unstable with respect to transverse undulations in the presence of a superflow. These undulations quickly transform into large primary vortex loops which then separate themselves from the interface. Simultaneously, a large number of small secondary vortex-antivortex nuclei are created in the supercooled region by fluctuations, resembling the conventional KZ mechanism. The primary vortex loops screen out the superflow in the inner region causing the annihilation of the secondary vortex-antivortex nuclei. The number of the *survived* secondary vortex loops is thus much smaller than that anticipated from the KZ conjecture. The dynamics of the vortex-loop evolution at very long times after the quench is studied numerically. We find that the number of vortex loops in the bulk of the supercooled region decays with time as $1/t$ which complies with the complete screening of superflow.

The structure of the paper is as follows. In Sec. II we formulate the TDGL model for ^3He . Section III describes the results of three-plus-one and two-plus-one-dimensional numerical simulations of the generalized TDGL model. In Sec. IV we present analytical studies of the NS interface instability. An estimate for the number of vortex loops created as a result of the NS interface instability is presented in Sec. V. Section VI treats the long-term dynamics of vortices in the transient state. The results of weakly nonlinear analysis of the interface instability are presented in Appendix B.

II. MODEL

In our calculations we use the simplest time-dependent description, namely the TDGL model with a scalar order parameter ψ . There are two major assumptions behind this model. First, we expect that a complex scalar order parameter is sufficient to describe vortex dynamics and vortex nucleation in $^3\text{He-B}$ at least not too close to the $A-B$ transition line.^{3,4} Approximation of the $^3\text{He-B}$ order parameter structure by a complex scalar ignores the actual rich structure of the nine-component complex order parameter specific for superfluid ^3He . Of course, we are thus unable to differentiate between various types of vortices that can exist in superfluid ^3He and to follow all kinds of transitions between them. However, we believe that this model gives a correct qualitative account for vortex dynamics. Certainly, this consider-

ation cannot describe properly the exact quantitative values of the vortex mutual-friction parameters which depend on ^3He -specific structure of the vortex cores. The other assumption concerns the nature of the TDGL model itself. This model seems to be a reasonable description for $^3\text{He-B}$ very close to T_c . It is expected to be exact in the so-called gapless regime when the order-parameter magnitude is smaller than the quasiparticle relaxation rate (for ^3He , the corresponding temperature range is, unfortunately, beyond the reach of present experiments). Moving away from T_c , kinetics of excitations becomes important, so that a description that employs the order parameter as the only relevant variable breaks down. For a vortex dynamics, in particular, a different feature becomes important: a nondissipative force on a moving vortex appears perpendicular to the vortex velocity in addition to a dissipative viscous force. The dissipative force is, in principle, taken care of by a simple TDGL model.¹⁰ To account for a nondissipative dynamics we allow for a complex relaxation rate of the order parameter in the TDGL equation. An imaginary part of the relaxation constant is known to result in a transverse force on vortices in superconductors.^{11,12} We write our starting equations in the form

$$(1 - i\eta)\partial_t\psi = \Delta\psi + [1 - f(\mathbf{r}, t)]\psi - |\psi|^2\psi + \zeta(\mathbf{r}, t). \quad (1)$$

This equation interpolates between two extremes: close to T_c the parameter $\eta \rightarrow 0$, which corresponds to the usual TDGL model, while large η corresponds to low temperatures. The latter case resembles the dissipationless Gross-Pitaevskii equation devised originally for a weakly interacting Bose gas at $T=0$ and then applied also for superfluid helium II at low temperatures.^{13,14}

Here f describes local temperature evolution. Since the energy released due to relaxation of the order parameter ψ is very small in Fermi superfluids, especially near T_c , because only a small fraction of particles participate in paired condensate, we can consider evolution of temperature independent on the order-parameter dynamics.

In Eq. (1), Δ is the three-dimensional (3D) Laplace operator, and distances and time are measured in units of the coherence length $\xi(T_\infty)$ and the characteristic time $\tau_{\text{GL}}(T_\infty)$, respectively. These quantities are taken at temperature T_∞ far from the heated bubble. For a Fermi liquid, the microscopic values of the Ginzburg-Landau parameters are

$$\tau_{\text{GL}}(T_\infty) = \pi\hbar/8(T_c - T_\infty),$$

the coherence length is

$$\xi(T) = \xi_0 \left(\frac{7\zeta(3)}{12(1 - T/T_c)} \right)^{1/2}, \quad \xi_0 = \frac{\hbar v_F}{2\pi T_c}.$$

Close to T_c the local temperature is controlled by normal-state heat diffusion and evolves as

$$f(\mathbf{r}, t) = \frac{T - T_\infty}{T_c - T_\infty} = \frac{E_0 \exp(-r^2/\sigma t)}{t^{3/2}}, \quad (2)$$

where σ is the normalized diffusion constant $\sigma = [48/7\zeta(3)][D\tau_0/\xi_0^2] \sim l/\xi_0$, where $\tau_0 = \pi\hbar/8T_c$. Here D is the usual diffusion constant, while l is the quasiparticle mean free path. In ^3He , σ is very large because $l \gg \xi_0$. E_0 determines the initial temperature of the hot bubble and is proportional to the deposited energy \mathcal{E}_0 such that

$$E_0 = \mathcal{E}_0 [C(T_c - T_\infty)\xi^3(T_\infty)(\pi\sigma)^{3/2}]^{-1},$$

where C is the heat capacity. Since the deposited energy is large compared to the characteristic superfluid energy, we assume $E_0 \gg 1$. Representative values of E_0 in our calculations are of the order of 30–50. An important parameter is a time $t_{\text{max}} = E_0^{2/3}$ at which the temperature in the center of the hot bubble drops down to T_c .

The Langevin force ζ with the correlator

$$\langle \zeta(\mathbf{r}, t)\zeta(\mathbf{r}', t') \rangle = 2T_f \delta(\mathbf{r} - \mathbf{r}') \delta(t - t')$$

describes thermal fluctuations with a strength T_f that corresponds to the heat bath temperature T_c (see the review Ref. 15 for detail). The effective noise strength in reduced units is

$$T_f = [27/7\zeta(3)\pi^4]^{1/2} \text{Gi}^{-1} [1 - (T/T_c)]^{-1/2},$$

where $\text{Gi} = \nu(0)\xi_0^3 T_c \sim 10^4$ is the Ginzburg number, $\nu(0)$ is normal density of states. This value of T_f results from the microscopic expression for the Ginzburg-Landau free energy of a Fermi superfluid with a scalar order parameter (see, for example, Ref. 16). We neglect dependence of T_f on the local temperature in what follows.

III. RESULTS OF SIMULATIONS

We solved Eq. (1) by the implicit Crank-Nicholson method. The integration domain was equal to 150^3 units of Eq. (1) with 200^3 mesh points. The computations were performed on massive parallel computer at Argonne National Laboratory. The boundary conditions were taken as $\partial\psi/\partial z = ik\psi$ with a constant k at the top and the bottom of the integration domain. This implies a uniform superflow $j_s = k|\psi_0|^2$ along the z axis far away from the temperature bubble, and the equilibrium value of the order parameter ψ_0 is related to k as follows: $|\psi_0|^2 = 1 - k^2$.

Consider first simulations for fully dissipative case with $\eta=0$. Selected results are shown in Fig. 1. The ‘‘explosion’’ (heat pulse) was created at $t=0$ at the origin located at the center of each panel in Fig. 1. One sees from Figs. 1(a)–(c) that without fluctuations (numerical noise only¹⁷) the vortex loops nucleate upon the passage of the thermal front. Not all of the loops survive: small loops collapse and only big ones grow. This type of behavior is characteristic for the vortex motion in a dissipative environment described by the TDGL equation with $\eta=0$:¹³ a single vortex ring in the presence of uniform superflow either shrink or expand depending on the circulation. For $\eta \neq 0$ the vortex ring also drifts parallel superflow direction.¹⁸ Although the vortex lines are centered around the point of the quench, they exhibit a certain degree of entanglement. After a long transient period, most of the vortex loops reconnect and form the almost axisymmetric configuration.

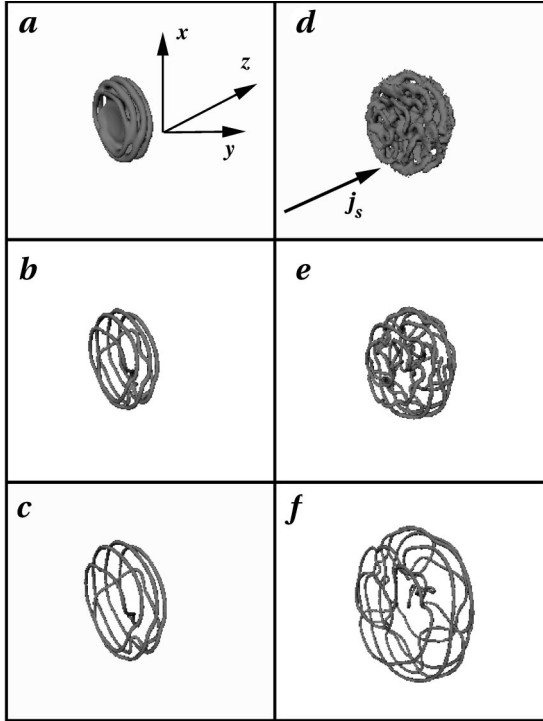


FIG. 1. 3D isosurface of $|\psi|=0.4$ for $\sigma=400$, $E_0=30$, and $k=0.5$. (a)–(c) $T_f=0$. Images are taken at times $t=36, 48, 80$. (d)–(f) $T_f=0.002$, $t=24, 48, 80$.

We find that the fluctuations have a strong effect at early stages: vortices nucleate not only at the normal-superfluid interface (we call them “primary” vortices), but also in the bulk of the supercooled region (“secondary” vortices), see Figs. 1(d) and (e). However, later on, small vortex loops in the interior collapse and only larger primary vortices survive and expand [Fig. 1(f)].

To elucidate the details of nucleation we considered a quasi-three-dimensional axisymmetric version of Eq. (1) depending on only r and z coordinates,

$$\Delta = \partial_r^2 + (1/r)\partial_r + \partial_z^2. \quad (3)$$

The domain was 500^2 with 1000^2 mesh points. We have found that without thermal fluctuations vortices nucleate at the front of the NS interface [black/gray border in Fig. 2(a)] analogous to the previous nonaxisymmetric case. Note that black areas on Figs. 2(a), (d), and also Fig. 3(a) correspond already to supercooled normal regions ($T < T_c$). The initial instability is seen as a corrugation of the interface. The interface propagates towards the center, leaving the vortices behind. As thermal fluctuations are turned on, the vortex loops also nucleate in the bulk of the supercooled region [black spot in Fig. 2(d)] resulting in the creation of the secondary vortex-antivortex pairs. We have found that primary vortices prevent the supercurrent from penetrating into the region filled with the secondary vortices. One sees that the primary vortices encircle the brighter spots in Figs. 2(b), (c), (e), and (f) indicating a larger value of the order parameter and thus a smaller value of the supercurrent. As a result the

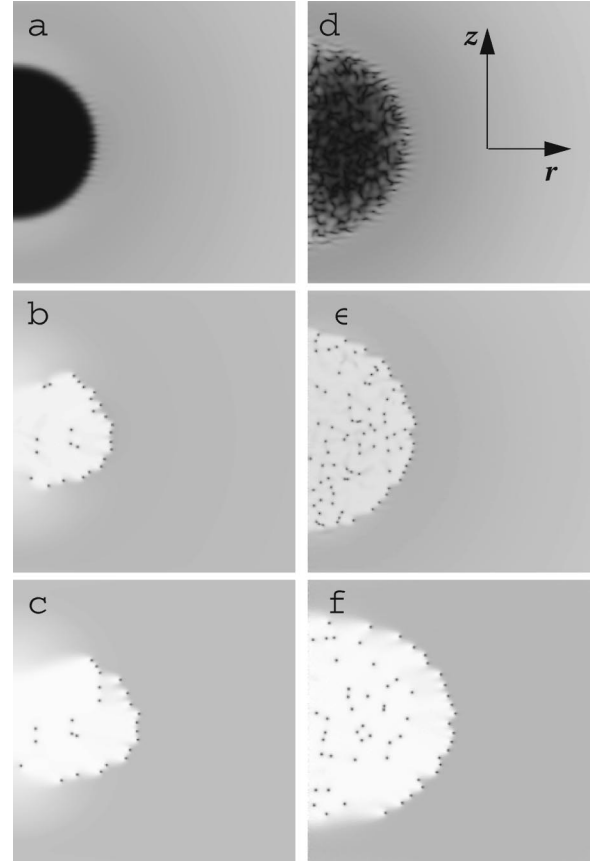


FIG. 2. Images of $|\psi|$ for axisymmetric Eq. (1) for $\sigma=5000$, $E_0=50$, and $k=0.5$, black corresponds to $|\psi|=0$ and white to $|\psi|=1$; gray ($|\psi|\sim 0.8$) indicates suppression of order parameter by current. Current is along the z axis. Vortices are seen as black dots. (a)–(c) $T_f=0$, images are shown for $t=40, 100, 200$; (d)–(f) $T_f=0.002$, for $t=30, 50, 200$.

secondary vortices either annihilate with antivortices due to their mutual attraction or collapse due to the absence of the inflating superflow.

Numerical solution of Eq. (1) with nonzero $\eta=0.5$ shows close similarity with previous results; see Fig. 3. However, in contrast to the case $\eta=0$, for a nonzero η the shape of the resulting vortex configuration is asymmetric in the direction of applied current. This is due to oblique motion of the vortices with respect to the current direction: For $\eta \neq 0$ the vortex loop not only changes its size but also drifts in the direction of superflow (see Ref. 18 for detail). Similar behavior occurs for $\eta \gg 1$. Our simulations performed for $\eta=5$ demonstrate that the superflow is expelled from the region surrounded by primary vortex loops: the order parameter is depressed considerably by the flow pattern around the region of the primary vortices. Thus the presence of the transverse force on vortices resulting from an imaginary part of the relaxation constant does not change qualitatively the mechanism of vortex formation and evolution during a rapid thermal quench.

We now summarize the main results of the numerical 3D+1 simulations. (i) Without fluctuations, vortices are nucleated at the interface between the superfluid and normal

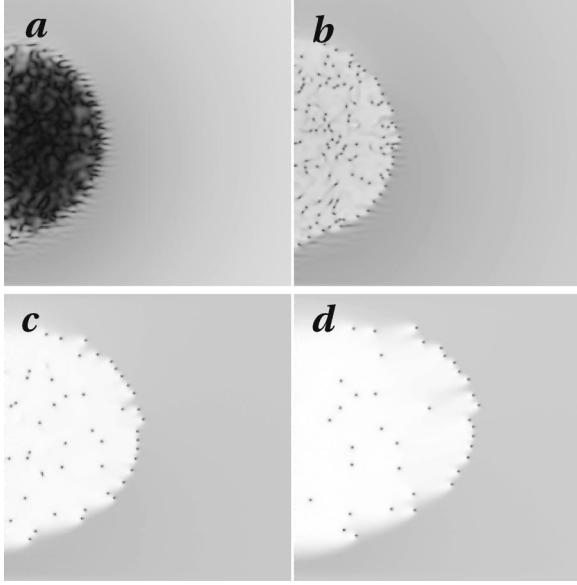


FIG. 3. Images of $|\psi|$ obtained by numerical solution of axisymmetric Eq. (1) for $\eta=0.5$. Other parameters are $E_0=50$, $\sigma=5000$, $k=0.5$, $T_f=0.002$. Images are shown for time $t=30$ (a), $t=40$ (b), $t=150$ (c), and $t=300$ (d).

phases (primary vortex loops). These vortices survive the collapse of the interface and remain in the superfluid phase after the cooling process is completed. (ii) Fluctuations produce vortex loops also inside the supercooled bubble (secondary vortices); however, these vortices disappear on later stages of the process. (iii) The supercurrent inside the region surrounded by primary vortex loops is considerably smaller than outside this region which is seen as brighter interior regions in Figs. 1–3. (iv) Primary vortex loops expand and move very slowly away from the place where they have been formed. Indeed, as seen from Figs. 1–3, vortices move only slightly during the time span of a decade from 30 to 300 units. We discuss these results in more detail in the following sections of the paper.

IV. INSTABILITY OF THE NORMAL-SUPERFLUID INTERFACE

Our numerical simulations shown in Figs. 1–3 indicate that nucleation of vortices happens predominantly within a relatively narrow region at the NS interface. The fact that vortices are nucleated there even without fluctuations suggests that the interface becomes unstable. In this section we perform the stability analysis and demonstrate that the interface indeed develops an instability towards the formation of vortices.

Following Refs. 3, 8, and 9, we expand the local temperature $1-f$ near T_c . Let us put $x=r_c-r$ where r_c is the radius of the surface at which $T=T_c$ or $f(r_c, t_c)=1$, i.e., $r_c^2=(3/2)\sigma t_c \ln(t_{\max}/t_c)$. A positive x is directed towards the hot region. We write $1-f(r, t) \approx -\alpha[x-v(t-t_c)]$, where

$$\alpha = -[\partial f / \partial r]_{f=1} = 2r_c / \sigma t_c$$

is the local temperature gradient and $v=(\alpha\tau_Q)^{-1}$ is the temperature front velocity defined through the quench rate $\tau_Q^{-1} = -[\partial f / \partial t]_{f=1}$. We have for the front velocity $v = -dr_c(t_c)/dt_c = (3\sigma t_c - 2r_c^2)/4r_c t_c$. The front starts to move towards the center at $t > t_* = t_{\max}/e$ and disappears at $t = t_{\max}$ when the temperature drops below T_c . The front velocity accelerates as the hot bubble collapses. Since its radius r_c is large compared to the coherence length, the temperature front can be considered flat. We choose the coordinates y, z parallel to the front. In a two-dimensional problem the solution is assumed independent of y .

We transform to the frame moving with the velocity v and perform the scaling of variables

$$\tilde{x} = vx, \tilde{z} = vz, \tilde{t} = tv^2, \quad (4)$$

$$\tilde{\psi} = \psi/v, u = v^3/\alpha. \quad (5)$$

We drop tildes in what follows. If the radius of the hot bubble R large comparing with coherence length ξ , which is the case for large deposited energies, one can neglect the curvature of the hot bubble. Therefore $\Delta \approx \partial_x^2 + \partial_z^2$, and Eq. (1) takes the form

$$(1-i\eta)\partial_t\psi = \Delta\psi + (1-i\eta)\partial_x\psi - \frac{x}{u}\psi - |\psi|^2\psi. \quad (6)$$

The parameter $u \sim (\sigma^2/t_{\max})/\ln^2(t_{\max}/t)$ is the only parameter of the problem (in addition to η); it characterizes the quench rate. For thermal diffusion in ^3He , the parameter u is large due to a large magnitude of σ . We discuss the physical meaning of u in more detail in Sec. IV A.

A. Steadily moving interface

Consider first a dissipative system with $\eta=0$. Equation (6) admits a family of stationary current-carrying solution

$$\psi = F(x)\exp(ikz) \quad (7)$$

with amplitude F satisfying the equation

$$\partial_x^2 F + \partial_x F - \left(\frac{x}{u} + k^2 \right) F - F^3 = 0. \quad (8)$$

We solved Eq. (8) numerically, using matching-shooting algorithm with Newton iterations from NAG library. The solutions to Eq. (8) for various values of u are shown in Fig. 4. As one sees from the figure, the supercooled normal region with $T < T_c$ expands with increase of u . A large- u limit for the stationary solution was studied in Ref. 8.

One can obtain an approximate solution to Eq. (8) for $u \gg 1$. Let us put

$$x = \bar{x} - u\gamma - uk^2, \quad (9)$$

where γ is to be determined later. For not very large \bar{x} one can neglect \bar{x}/u in Eq. (8) to get the equation

$$\partial_x^2 F_0 + \partial_x F_0 + \gamma F_0 - F_0^3 = 0 \quad (10)$$

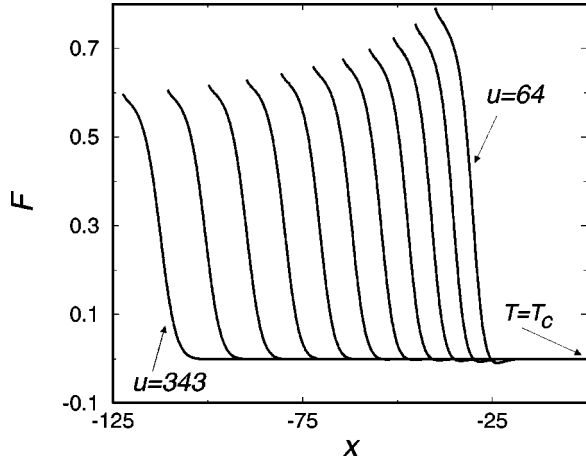


FIG. 4. The steady NS interface F vs x for different values of u . The ternal front $T=T_c$ is at $x=0$ and is moving to the right.

for an approximate interface solution F_0 . The interface $F_0(\bar{x})$ connects the two equilibria $F = \pm\sqrt{\gamma}$ and $F=0$; see Fig. 5. The function F_0 approximates the exact solution F to Eq. (8) fairly well for not very large \bar{x} . For large negative $\bar{x} \ll u$, the solution should be replaced by its final asymptotics $F = \sqrt{\gamma - \bar{x}/u}$. For large positive \bar{x} , the solution of Eq. (10) should be matched with the true asymptotics for $F \rightarrow 0$ found from Eq. (8). It is given by the expression

$$F \sim \exp(-\bar{x}/2) \text{Ai}[u^{2/3}(\gamma - 1/4 - \bar{x}/u)]. \quad (11)$$

As it was shown in Ref. 8, for $u \rightarrow \infty$ the matching is possible for $\gamma \rightarrow 1/4$. Indeed, for large \bar{x} , one has for the Airy function

$$\text{Ai}(-z) \sim z^{-1/4} \sin(\rho + \pi/4), \quad (12)$$

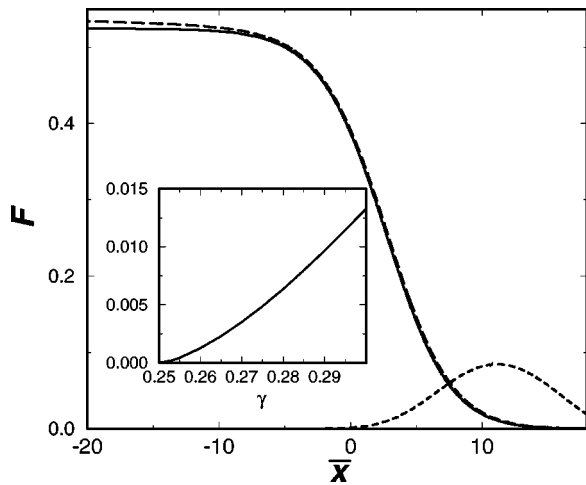


FIG. 5. Solution to Eq. (10) for $\gamma=0.275$ (solid line). For comparison is show solution for Eq. (8) for $u=1728$ (long dashed line). Short-dashed line shows $F_0^2 \exp(x)$. Inset: the ratio of integrals $\int_{-\infty}^{\infty} F_0^4 e^x dx / \int_{-\infty}^{\infty} F_0^2 e^x dx$ as a function of γ , to be used in Appendix A.

where $\rho = 2/3z^{3/2}$, and $z = u^{2/3}(\Omega^2 - \bar{x}/u)$ while $\Omega = \sqrt{\gamma - 1/4}$. Expanding ρ for $\bar{x}/u \ll 1$ one obtains from Eq. (11)

$$F \sim \exp(-\bar{x}/2) \sin\left(\frac{2}{3}u\Omega^3 + \frac{\pi}{4} - \Omega\bar{x}\right). \quad (13)$$

On the other hand, Eq. (10) gives for small F_0 ,

$$F_0 = C \exp(-\bar{x}/2) \sin(\Omega\bar{x} + \phi), \quad (14)$$

where C and ϕ are constants. The function F_0 , of course, is independent of u , and the constant ϕ cannot be large. Matching of Eqs. (13) and (14) thus requires $\Omega \rightarrow 0$ where $\gamma = 1/4 + O(u^{-2/3})$.

The same consideration applies also for a complex relaxation constant $\eta \neq 0$. We now put in Eq. (6)

$$\psi = F(x) \exp(ikz + i\omega t + i\kappa x), \quad (15)$$

where ω and κ are the frequency and longitudinal wave number which will be defined later. One sees that an interesting feature for any $\eta \neq 0$ is the emission of oblique waves from NS interface. Substituting Eq. (15) into Eq. (6) one obtains

$$\begin{aligned} & i\omega(1-i\eta)F - (1-i\eta)(\partial_x F + i\kappa F) \\ & = \partial_x^2 F + 2i\kappa \partial_x F - \left(\frac{x}{u} + k^2 + \kappa^2\right) F - F^3. \end{aligned} \quad (16)$$

Fixing

$$\kappa = \eta/2, \omega = \kappa = \eta/2 \quad (17)$$

one derives Eq. (8) with the k^2 replaced by $k^2 + \kappa^2$, which can be excluded by a proper shift of x .

The coordinate transformation Eq. (9) determines the position of the interface as a function of the quench parameter u . With an increase in u , the interface shifts to negative x leaving a supercooled normal region with $T < T_c$ behind as seen in Fig. 4. The size of the supercooled region is $\delta r \sim u/v$ in the GL units. The growth of fluctuations is described by linearized Eq. (1):

$$\partial_t \psi = (t/\tau_Q) \psi.$$

The fluctuation grows exponentially with a characteristic Zurek time $\tau_Z \sim \tau_Q^{1/2}$. According to Eq. (1), the coherence length decreases with decreasing temperature and reaches the characteristic Zurek length at $\xi_Z \sim \tau_Q^{1/4}$ at this time. Topological defects can be created by fluctuations if the size of the supercooled region δr is considerably larger than ξ_Z . The estimate gives $\delta r/\xi_Z \sim u/v \tau_Q^{1/4} \sim u^{3/4}$. Therefore fluctuation can produce vortices during such a phase transition only if the condition of a rapid quench $u \gg 1$ is satisfied.⁴ We shall see now that the same condition determines an instability of the interface in presence of a supercurrent towards formation of vortices. Thus at a rapid transition with $u \gg 1$ two processes take place simultaneously: formation of vortices at the

interface between the superfluid and normal supercooled region and creation of vortices by fluctuations inside the normal region.

B. Linear analysis

Let us examine the transverse stability of stationary solution to Eq. (6). For $\eta=0$ we put $\psi=[F+w(x,z,t)]\times\exp(ikz)$, where w is a perturbation. For the function w we derive from Eq. (6)

$$\begin{aligned} \partial_t w = \partial_x^2 w + \partial_z^2 w + 2ik\partial_z w + \partial_x w - \left(\frac{x}{u} + k^2\right)w \\ - F^2(2w + w^*) - F(2|w|^2 + w^2) - |w|^2 w. \end{aligned} \quad (18)$$

Separating real and imaginary parts of $w = a + ib$ one has

$$\begin{aligned} \partial_t a = \partial_x^2 a + \partial_z^2 a - 2k\partial_z b + \partial_x a - \left(\frac{x}{u} + k^2\right)a - 3F^2 a \\ - F(3a^2 - b^2) - (a^2 + b^2)a, \end{aligned} \quad (19)$$

$$\begin{aligned} \partial_t b = \partial_x^2 b + \partial_z^2 b + 2k\partial_z a + \partial_x b - \left(\frac{x}{u} + k^2\right)b - F^2 b - 2Fab \\ - (a^2 + b^2)b. \end{aligned} \quad (20)$$

Dropping nonlinear terms in a, b and representing the solution to Eqs. (19) and (20) in the form

$$\begin{pmatrix} a \\ b \end{pmatrix} = \begin{pmatrix} A \\ iB \end{pmatrix} \exp(\lambda(q)t + iqz), \quad (21)$$

where q is the transverse undulations wave number and λ is the growth rate, we obtain ($\chi = kq, \Lambda = \lambda + q^2$)

$$\begin{aligned} \Lambda A + 2\chi B = \partial_x^2 A + \partial_x A - (x/u + k^2)A - 3F^2 A, \\ \Lambda B + 2\chi A = \partial_x^2 B + \partial_x B - (x/u + k^2)B - F^2 B. \end{aligned} \quad (22)$$

In the case of a complex relaxation constant perturbative solution to Eq. (6) is sought in the form $\psi = (F + w)\exp(ikz + i\omega t + i\kappa x)$. Substituting this ansatz into Eq. (6) one obtains Eq. (22) where k^2 is replaced with $k^2 + \kappa^2$, and $\chi = kq - i\lambda\eta/2$. Therefore all the results on linear stability can be easily carried over to the case of arbitrary η .

Solution to Eqs. (22) can be obtained numerically for arbitrary u and χ . Moreover, one can find analytical solutions in two limits: long-wavelength limit $\chi \ll 1$ and large-velocity limit $u \gg 1$.

C. Long-wavelength limit

The eigenvalue Λ for $\chi \rightarrow 0$ can be found as an expansion in χ : $\Lambda = \chi\Lambda_1 + \chi^2\Lambda_2 + \dots$ and similarly for A and B . Within the zeroth order in χ , the second Eq. (22) coincides with the equation for the stationary solution Eq. (8). One has $A_0 = 0, B_0 = F$. Within the first order, we derive $B_1 = 0$ and

$$\partial_x^2 A_1 + \partial_x A_1 - (x/u + k^2)A_1 - 3F^2 A_1 = 2F. \quad (23)$$

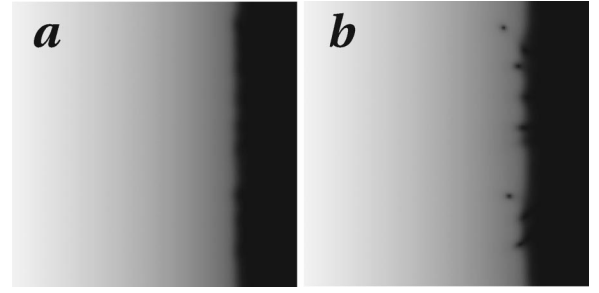


FIG. 6. Images of $|\psi|$ obtained by numerical solution of Eq. (6) for $u = 100, k = 0.1$, size of the integration domain 240×240 , number of grid points 400×400 , images are shown for $t = 90$ (a), $t = 125$ (b).

The solution $A_1 = 2u\partial_x F$ is obtained by differentiating Eq. (8). The second-order terms in Eq. (22) give

$$\partial_x^2 B_2 + \partial_x B_2 - (x/u + k^2 + F^2)B_2 = 4u\partial_x F + \Lambda_2 F. \quad (24)$$

A zero mode of Eq. (24) is F . Equation (24) is not self-adjoint, therefore the adjoint zero mode B^\dagger does not coincide with F . The corresponding adjoint operator has the form

$$\partial_x^2 B^\dagger - \partial_x B^\dagger - (x/u + k^2 + F^2)B^\dagger = 0. \quad (25)$$

One checks by substitution that function $B^\dagger = F \exp(x)$ satisfies Eq. (25). Equation (24) has a solution if the orthogonality condition with respect to the zero mode is fulfilled

$$\int_{-\infty}^{\infty} dx F e^x (4u\partial_x F + \Lambda_2 F) = 0. \quad (26)$$

After integration we obtain $\Lambda_2 = 2u$. Returning to the original notations, we obtain the *exact* result

$$\lambda = q^2(2uk^2 - 1) + O(q^4). \quad (27)$$

For $\eta \neq 0$ we obtain an implicit condition for the instability growth rate:

$$\lambda = 2u(kq - i\lambda\eta/2)^2 - q^2. \quad (28)$$

It is easy to check that the threshold is given by the condition $2k^2u = 1$ irrespectively of η . The growthrate λ near the threshold $2k^2u - 1 \rightarrow 0$ is [compare with Eq. (27)]

$$\lambda \approx q^2 \frac{2uk^2 - 1}{1 - i2u\eta kq}. \quad (29)$$

The instability occurs above the threshold $k_v^2 = (2u)^{-1}$ or

$$k_v^2 \sim \alpha^{2/3}/u^{1/3} \sim \sigma^{-1} \ln(t_{\max}/t)$$

in the Ginzburg–Landau units. The threshold is much smaller than the bulk critical value $k_c = 1/\sqrt{3}$ for a rapid quench $u \gg 1$; it can be exceeded for a very small superflow.

To visualize the outcome of instability and to demonstrate that it indeed leads to formation of vortices we performed numerical simulations using Eq. (6). The results are presented in Fig. 6. They clearly show that the instability results in nucleation of vortices at the interface.

D. Large- u limit

The instability threshold obtained above does not provide the optimal wave number q_{\max} for the most unstable perturbation. This wave number can be found by evaluating higher-order terms in $\lambda(q)$ up to q^4 , which will provide the fall off of the growth rate. A full analytical solution of the set of Eqs. (22) can be obtained in the limit of a large u (fast quench rate). Let us start first with $\eta=0$ and consider the large- u limit in more detail. In this limit one assumes $\Lambda \sim \chi \sim 1/u$. Let us put again $x = \bar{x} - u\gamma - uk^2$ in Eqs. (22). For $u \gg 1$ we treat the terms containing Λ , χ , and \bar{x}/u as perturbations. The steady-state solution of Eq. (8) should also be written within the same accuracy. Therefore, we use the approximate solution F_0 of Eq. (10) as discussed above. In general, the interface has a form $F_0(\bar{x} - x_0)$ where x_0 is an arbitrary constant determining the position of the interface. The position x_0 is fixed by the corresponding solvability condition, see below.

Having established the properties of the steady-state solution to Eq. (10), we turn to the stability analysis of the set of Eqs. (22). In the large- u limit these equations assume the form

$$\begin{aligned} \Lambda A + 2\chi B + \epsilon x A &= \partial_x^2 A + \partial_x A + \gamma A - 3F_0^2 A, \\ \Lambda B + 2\chi A + \epsilon x B &= \partial_x^2 B + \partial_x B + \gamma B - F_0^2 B. \end{aligned} \quad (30)$$

We omit the bar over x for brevity.

For $\epsilon=0$ Eqs. (30) have zero modes: $(A, B) = (0, F_0(x - x_0))$, similar to Eqs. (22). In addition, Eq. (30) has an extra zero mode $(A, B) = (F_0'(x - x_0), 0)$ that manifests the translation invariance for $\epsilon=0$ (we put $F_0' \equiv \partial F_0 / \partial x$). For any $\epsilon \neq 0$ the translation invariance is broken by the perturbation $\sim x/uA$, x/uB in the left-hand side of Eqs. (30). The corresponding solvability condition will specify the value of x_0 .

In contrast to the case of $\chi \rightarrow 0$ considered in the previous section, the solvability conditions must be fulfilled simultaneously for both zero modes of Eq. (30). Thus representing the general zero-mode solution of Eq. (30) at the zeroth order in the form

$$\begin{pmatrix} A \\ B \end{pmatrix} = \begin{pmatrix} a_0 F_0'(x - x_0) \\ b_0 F_0(x - x_0) \end{pmatrix}, \quad (31)$$

where a_0, b_0 are arbitrary constants, and performing the integrations with the corresponding zero modes, one obtains characteristic equation for Λ :

$$\Lambda^2 + \frac{1}{u} c_1 \Lambda - 4c_2 \chi^2 + \frac{d}{u^2} = 0, \quad (32)$$

where the coefficients $c_{1,2}, d$ are given in the forms of integrals of F with the corresponding zero modes in the interval $-\infty < \bar{x} < \infty$:

$$c_1 = \frac{1}{u} (i_5/i_2 + i_4/i_1), \quad c_2 = \frac{i_3^2}{i_1 i_2}, \quad d = \frac{i_4 i_5}{u^2 i_1 i_2}, \quad (33)$$

where

$$\begin{aligned} i_1 &= \int_{-\infty}^{\infty} F_0^2 e^x dx, \quad i_2 = \int_{-\infty}^{\infty} (F_0')^2 e^x dx, \\ i_3 &= \int_{-\infty}^{\infty} F_0 F_0' e^x dx = -i_1/2, \\ i_4 &= \int_{-\infty}^{\infty} (x - x_0) F_0^2 e^x dx, \\ i_5 &= \int_{-\infty}^{\infty} (x - x_0) (F_0')^2 e^x dx. \end{aligned} \quad (34)$$

It should be noted that for $\bar{x} \rightarrow \infty$ the asymptotic tail of the function F_0 is incorrect. However, as already mentioned, the crossover to this asymptotic behavior occurs when F_0 is already very small; see Fig. 5.

The constant x_0 is determined from the requirement that Eqs. (30) always have an eigenvalue $\Lambda = 0$ for $\chi = 0$ as was also the case for the original Eqs. (22). It implies that $i_4 = 0$ and fixes the value of x_0 ,

$$x_0 = i_1^{-1} \int_{-\infty}^{\infty} (F_0')^2 e^x dx. \quad (35)$$

Evaluation of the integrals in Eqs. (34) for $\gamma \rightarrow 1/4$ yields

$$c_1 = \frac{2}{u}, \quad c_2 = 1 \quad (36)$$

(see Appendix A for details). Substitution of Eq. (36) into Eq. (32) results in

$$\Lambda = \pm \sqrt{1/u^2 + 4\chi^2} - 1/u. \quad (37)$$

Returning to the original definitions, we have an explicit expression for the largest eigenvalue of the transverse instability,

$$\lambda = \sqrt{1/u^2 + 4k^2 q^2} - 1/u - q^2. \quad (38)$$

For $u \rightarrow \infty$ one has from Eq. (38) $\lambda = 2|kq| - q^2$. The maximum growthrate is achieved at $q_{\max} = k$ and is simply k^2 . Numerical solution of Eqs. (22) demonstrates an excellent agreement with the theoretical expression Eq. (38); see Fig. 7.

In case of a nonzero η , Eq. (37) gives for $u \gg 1$,

$$\lambda(1 - i\eta) = 2|kq| - q^2.$$

Again, the real part of the growth rate has a maximum at $q_{\max} = k$. Stability analysis thus confirms the conclusion drawn in Sec. III from the numerical results that the NS interface becomes unstable irrespectively of the imaginary part of the relaxation constant. In our model this is equivalent to the conclusion that the instability is not limited to a vicinity of the critical temperature but exists for any temperatures.

Very close to the threshold of the instability, there is a possibility that the solution remains finite due to nonlinear terms in Eqs. (19) and (20). Nonlinearity may create a finite

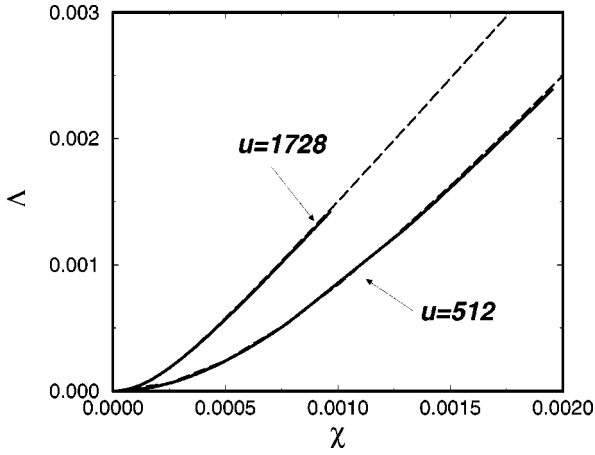


FIG. 7. Λ vs χ for $u=512$ and $u=1728$, solid lines show results of numerical solution of Eq. (22), dashed lines represent analytical solution Eq. (37).

barrier that a perturbation has to overcome to initiate the instability. Nonlinear stability analysis described in Appendix B shows that the dynamics of the system close to the instability threshold is governed by the so-called Kuramoto-Sivashinsky equation (KSE) known in the theory of pattern formation and interface growth models.^{19,20} It is known that KSE exhibits a variety of stable periodic²¹ as well as spatiotemporal chaotic solutions. For our case, this would imply persistent spatiotemporal dynamics at the interface *without nucleation of vortices*. However, moving away from the instability threshold overrides nonlinear terms and results in blowing up solutions, see, e.g., Ref. 22. We did not succeed yet to observe KSE-type dynamics in our simulations with Eq. (6) because it requires very large system sizes and very large times of integration due to the critical slowdown at the threshold of instability. As long as the experimental situation in ³He is concerned, the instability threshold is exceeded rapidly as the moving interface accelerates during the cool down. It would be interesting to verify KSE scenario in a specially designed experiment, e.g., with liquid crystals.

V. NUMBER OF CREATED VORTEX LOOPS

Now we apply the above results to estimate the number of vortex loops nucleated due to the interface instability. This is determined by the wave number of the most unstable mode. In the case of thermal quench, the velocity of the NS interface $u \rightarrow \infty$ as time approaches t_{\max} , therefore the limit of large u applies. The growth of perturbations near the interface is described by the Fourier integral

$$w \sim \int dq S(q) \exp[\lambda(q)t + iqz], \quad (39)$$

where $w(x, z, t)$ is the perturbation to the interface solution, $S(q)$ is the spectrum of initial perturbation. In the context of original problem described by Eq. (1) the velocity of the interface and therefore parameter u, k are certain functions of time, see Eqs. (4). Therefore instead of expression $\lambda(q)t$ in Eq. (39) one has to use an integral $\int_0^t \lambda(q(t')) dt'$, valid in

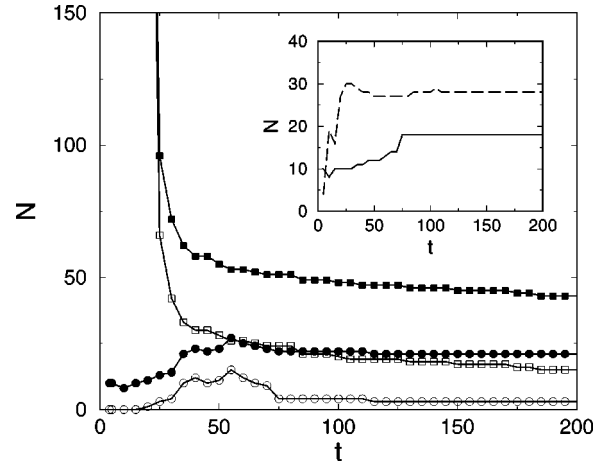


FIG. 8. Number of vortices N^+ (filled symbols) and antivortices N^- (open symbols) vs time for $\sigma=5000, E_0=50$, and $k=0.5$. Circles correspond to $T_f=0$ and squares to $T_f=0.002$. Inset: $N = N^+ - N^-$ for $T_f=0$ (solid line) and $T_f=0.002$ (dashed line).

the WKB approximation. However, in the large u limit this time dependence is canceled out trivially and one obtains again Eq. (39).

Taking into account that it is the thermal noise which provides initial perturbations for the interface instability w , and using saddle-point approximation for the integral in Eq. (39) for $t \gg 1$, one derives $\langle |w| \rangle \sim \sqrt{T_f} \text{Re} \exp[k^2 t + ikz]$. The number of vortices is estimated as $N = r_0 k$, where r_0 is the radius of the front where the perturbations $\langle |w| \rangle$ become of the order of unity. The time interval t_0 corresponding to $\langle |w| \rangle = 1$ is $t_0 \sim k^{-2} \ln(T_f^{-1})$. Vortices have no time to grow if $t_0 \rightarrow t_{\max}$. In this limit one finds $r_0^2 \sim \sigma(t_{\max} - t_0)$. The number of vortices is given by

$$N \sim k r_0 \sim \sqrt{\sigma k} \sqrt{t_{\max} - t_0}. \quad (40)$$

Taking into account that in our original notation $k \sim v_s/v_c$, where v_s and v_c are the imposed and critical GL superflow velocity, respectively, and $t_{\max} = E_0^{2/3}$, we arrive at

$$N \sim \sqrt{\sigma} E_0^{1/3} \sqrt{(v_s/v_c)^2 - \beta^2 \ln(T_f^{-1})/E_0^{2/3}}, \quad (41)$$

where $\beta = \text{const}$. Equation (41) exhibits a slow logarithmic dependence of the number of vortices at the interface on the level of fluctuations.

VI. DYNAMICS OF VORTEX-ANTIVORTEX ANNIHILATION

In this section we concentrate on the evolution of vortices created by both the instability and fluctuations. We will argue that the outcome of the interface instability determines the distribution of supercurrent around and inside the vortex. This distribution, in turn, determines the dynamics of primary vortex loops and the collapse of the secondary vortices.

Figure 8 shows the number of vortices N^+ and antivortices N^- vs time with and without fluctuations. Fluctuations initially create a very large number $\sim 10^4$ of vortices and antivortices in the bulk which then annihilate. The resulting

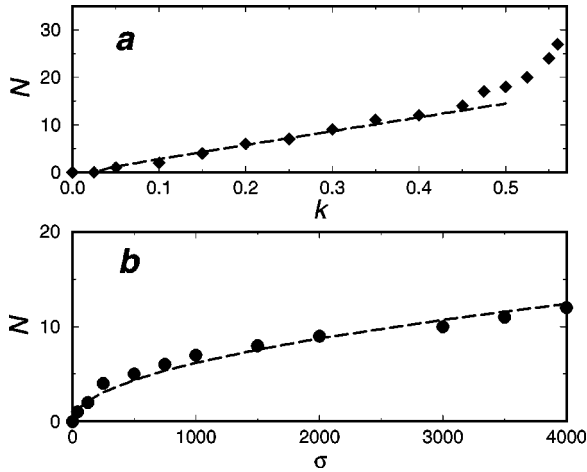


FIG. 9. (a) Number of survived vortex rings N as function of k for $E_0=50$ and $\sigma=5000$ and (b) N vs σ for $k=0.4$ and $E_0=50$. Dashed lines show fitting to prediction Eq. (41).

amount of surviving vortices $N=N^+-N^-$ is only weakly dependent on fluctuations.

Shown in Fig. 9 is the number of vortex loops N vs quench parameters and applied current k . At small k the number N shows threshold behavior while becoming almost linear for larger k values. The deviations from a linear law appear close to the critical value $k_c=1/\sqrt{3}$ for the flow instability in a homogeneous system, when vortices start to nucleate spontaneously everywhere in the bulk.

The estimate Eq. (41) is in agreement with the results of simulations,²³ see Fig. 9. For the experimental values of the parameters, our analysis results in about ten surviving vortices per heating event. It is consistent with Ref. 6 where as many as 6–20 vortices per neutron were detected.

Our simulations identify two distinct regimes of annihilation of vortices and antivortices vs time; see Fig. 8. First, a large number of vortices is created at early stages of the quench ($t < 50$ in Fig. 8). Then, this number decreases rapidly down to much smaller values. At a later stage ($t > 50$), it relaxes slowly towards the equilibrium value. We performed detailed numerical simulations in order to elaborate the statistics of the vortex annihilation at the later stages of the quench. The results are shown in Figs. 10 and 11. The simulations are performed for the quasi-three-dimensional geometry (assuming axial symmetry of the vortex-loop configuration) and also for a pure two-dimensional geometry (straight vortex lines).

Let us discuss first the results of simulations for zero applied current j_s . As one sees from Fig. 10, the behavior for both 2D and 3D situations is similar: a fast initial relaxation and then a slow decay consistent with the dependence $N \sim 1/t$ (in agreement with Ref. 24 for the homogeneous quench). This result complies with the mean-field theory of annihilation based on the assumption that the annihilation rate of vortices is proportional to the local density of anti-vortices:

$$dN^+/dt \sim -N^+N^-$$

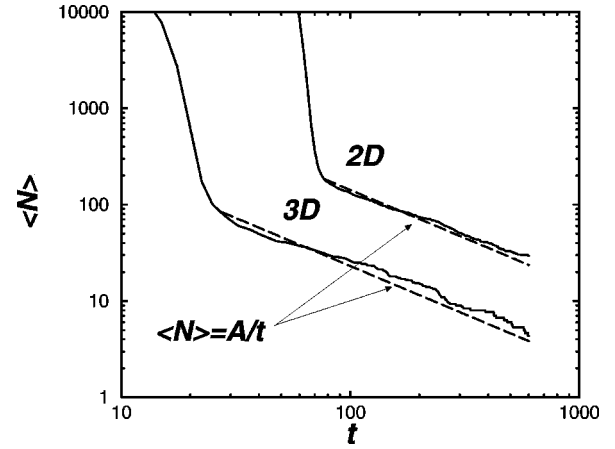


FIG. 10. Number of vortices N vs time for $k=0$ (zero supercurrent). Parameters of simulations: $E_0=50, \sigma=10\,000$, domain size 1000×1000 for quasi-three-dimensional sample (line 3D), and $E_0=50, \sigma=6000$, domain size 800×800 for the two-dimensional sample. Each line is averaged over five independent realization of thermal noise.

(Vinen's equation²⁵). Assuming $N^+=N^-$ one readily obtains $N^\pm \sim 1/t$. This behavior is in disagreement with Refs. 26 and 27 which claim that a long-range interaction between the vortices results in substantial deviation from the mean-field theory. A $1/t$ relaxation is well-established in experiments where the decay of vorticity was measured²⁸ after an abrupt stop of the rotating container with superfluid ^3He .

If the flow is applied ($k \neq 0$), one has in general $N^+ \neq N^-$. From the mean-field theory one immediately obtains an exponential relaxation $N^+ \sim \exp(-\alpha t) + B$, where B is a final number of vortices and α is a relaxation rate $\alpha \sim N^+ - N^-$. However, this results is in clear disagreement with the numerical simulations shown in Fig. 11. As it follows from the figure, the relaxation law is the same as in the previous case $k=0$, the only difference being that N^+ approaches an equilibrium value, $N^+ = A/t + B$.

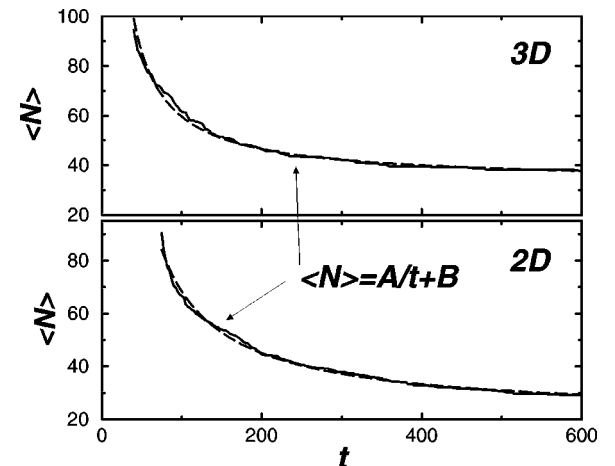


FIG. 11. Number of vortices N vs time $k=0.4$ for the three-dimensional sample and $k=0.3$ for the two-dimensional one. Other parameters the same as in Fig. 10. The limiting number of vortices is $B \approx 33.5$ in 3D and $B \approx 21.6$ in 2D.

Figure 11 gives a very strong evidence in favor of the conclusion that the supercurrent is expelled from the vortex region to the periphery, being screened out by vortices generated by the NS interface instability as seen from Figs. 2 and 3. The absence of supercurrent inside the vortex region recovers the mean-field behavior $N^+ \sim 1/t$ for the bulk vortices. Such an effective screening of the supercurrent can be understood in the following way. The number of created vortex loops is determined by the wave number q_{\max} that corresponds to the maximum growth rate. Since $q_{\max} = k$ the number of vortices is such that it exactly compensates the phase difference produced by the supercurrent along the interface. As a result, no net current remains inside the region surrounded by primary vortex loops.

Equation (41) $N \sim kr_0$ can also be written as $v_s \sim N\kappa/r_0$ which is the condition that a flow $k = mv_s$ supports an array of N vortex loops with a radius r_0 and a circulation $\kappa = \pi/m$. Therefore the vortices created at the interface are almost in equilibrium under the action of the superflow and of the linear tension. Their evolution is thus very slow (as can be seen also from Figs. 1–3). As a result, the loops created by fluctuations inside the supercooled bubble have enough time to shrink away and disappear before the primary loops grow and go far from the bubble, reducing the screening of superflow. This explains why the $1/t$ decay of vorticity persists for as long as 1000 time units in our simulations.

Both the analytical estimates Eq. (41) and the numerical results shown in Fig. 9(a) together with the long-term vorticity relaxation depicted in Fig. 11 strongly suggest that the overall number of nucleated vortices is determined primarily by the interface instability and is a linear function of the applied superflow, at least for superfluid velocities far from the bulk instability limit. This is the exact result of the TDGL model under the condition that cooling is accomplished by thermal diffusion. In the experiment,⁶ however, a dependence close to $N \propto v_s^3$ has been observed. The origin of the disagreement between the theoretical predictions and the experimental observations can be searched for both in the quality of the TDGL-model description and in the possible complications in interpreting the experimental results. From the theoretical side, the assumption of thermal diffusion for the mechanism of removal of the neutron-deposited energy is most vulnerable. In reality, formation of vortices could start before the excitations produced by the neutron absorption thermalize; the temperature thus would no longer be a good quantity at this stage of the vortex dynamics. Variations of pressure in course of the absorption of a neutron can also be an important factor initiating the phase transition. From the experimental side, one can think of effects of the container walls on the vortex nucleation. Indeed, the neutron absorption happens close to the wall so that the boundary of the hot bubble can approach the wall and initiate the vortex formation at nucleation sites at the wall. One more factor can be an effect of the bulk superflow instability. Indeed, Fig. 9(a) shows an upturn of the number of nucleated vortices as the superflow approaches the instability limit $k = 1/\sqrt{3}$. Superflow velocities in the experiment⁶ are not far from the critical value; this proximity can superimpose on the linear dependence and modify the behavior of the created vorticity. A

definite conclusion from this discussion is that more studies, both theoretical and experimental, are needed to clarify the nature of vortex formation at rapid second-order phase transitions.

VII. CONCLUSION

We have found that the rapid normal-superfluid transition in the presence of superflow is dominated by a transverse instability of the NS interface propagating from the bulk into the normal region. This instability produces primary vortex loops which then separate from the interface. Simultaneously, a large number of vortex-antivortex pairs are created by fluctuations in the bulk of the supercooled region formed after the collapse of the interface. Our numerical results indicate that the dynamics of vortex-antivortex annihilation in the bulk obeys a simple power law $N \sim 1/t$ irrespectively of the dimensionality of the space. Our numerical simulations show that the primary vortex loops screen out the superflow and cause annihilation of the vortex-antivortex pairs in the bulk. The number of surviving vortices is determined by superflow-dependent optimum wave vector of the interface instability.

We were able to derive analytically exact expressions for the instability threshold and for the growth rate of transverse perturbations in the limit of fast quench. We verified that this scenario remains valid also far away from the critical temperature where the dynamics of vortex nucleation is described by a modified TDGL model with a complex relaxation rate. We show that in the very vicinity of the threshold the dynamics of transverse undulations is described by the Kuramoto-Sivashinsky equation. Though our results are intended for interpretation of experiments⁶ with ³He, they can also be useful for nonlinear optical systems²⁹ and may stimulate new experiments, e.g., in liquid crystals.

ACKNOWLEDGMENTS

We are grateful to V. Eltsov, M. Krusius, G. Volovik, L. Kramer, L. Pismen, V. Steinberg, and W. Zurek for stimulating discussions. This research is supported by US DOE, grant W-31-109-ENG-38 and by Russian Foundation for Basic Research, grant 99-02-16043.

APPENDIX A: EVALUATION OF CONSTANTS IN EQ. (32)

To find the constants $c_{1,2}$ defined by Eq. (33) we need to express all integrals in Eqs. (34) in terms of i_1 . This is possible to achieve in the limit of $\gamma \rightarrow 1/4$. In this case the main contribution to the integrals (34) comes from the region where the function F_0 is already small, and we can drop nonlinearity in Eq. (10) in order to evaluate the function F_0 . For the constant c_2 one has from Eq. (34)

$$c_2 = i_1 / (4i_2). \quad (\text{A1})$$

The integral i_2 can be transformed by partial integration to the form

$$i_2 = \int_{-\infty}^{\infty} \left(\frac{1}{2} (F_0'')^2 - F_0 F_0'' \right) e^x dx. \quad (\text{A2})$$

Using Eq. (10) we substitute $F_0'' = -F_0' - \gamma F_0 + F_0^3$, and performing partial integration in Eq. (A2), we derive

$$i_2 = \gamma i_1 + \int_{-\infty}^{\infty} F_0^4 e^x dx. \quad (\text{A3})$$

However, the last integral in Eq. (A3) is very small comparing to i_1 for $\gamma \rightarrow 1/4$; see inset to Fig. 5. It follows from the fact that function $F_0^2 e^x$ has a maximum where the function F_0 is already very small; see Fig. 5. Indeed, the maximum of $F_0^2 e^x$ is determined by the condition $F_0'/F_0 = -1/2$, which implies that $F_0 \sim e^{x/2}$. Consequently, Eq. (10) provides $F_0 \sim e^{px}$, $p = -1/2 \pm i\sqrt{\gamma - 1/4}$ near the equilibrium $F_0 = 0$. Thus one sees that when $\gamma \rightarrow 1/4$ the maximum condition for $F_0^2 e^x$ is fulfilled at $F_0 \rightarrow 0$. Therefore for $\gamma \rightarrow 1/4$ we can neglect the last integral in Eq. (A3), leading to $i_2 = \gamma i_1$. Substituting it into Eq. (A1) gives $c_2 = 1$.

To calculate the constant c_1 we use that $i_4 = 0$ and exclude x_0 from i_5 with the help of Eq. (35). We have

$$c_1 = i_5 / i_2 = \frac{1}{\gamma i_1} \int_{-\infty}^{\infty} x (F_0')^2 e^x dx - \frac{1}{i_1} \int_{-\infty}^{\infty} x F_0^2 e^x dx. \quad (\text{A4})$$

Integrating by parts we find

$$\begin{aligned} \int_{-\infty}^{\infty} x (F_0')^2 e^x dx &= \int_{-\infty}^{\infty} \left(\frac{1}{2} (F_0'')^2 - F_0 F_0'' \right) x e^x dx \\ &= \int_{-\infty}^{\infty} \frac{1}{2} F_0^2 (x+2) e^x dx \\ &\quad + \int_{-\infty}^{\infty} (\gamma F_0^2 + F_0' F_0) x e^x dx \\ &= \gamma \int_{-\infty}^{\infty} x F_0^2 e^x dx + i_1 / 2. \end{aligned} \quad (\text{A5})$$

Substituting Eq. (A5) into Eq. (A4) one obtains $c_1 = 2$.

APPENDIX B: WEAKLY NONLINEAR ANALYSIS

In this section we consider effect of nonlinearity on the interface instability. The analysis is convenient to perform in the limit of $u \gg 1$. We generalize the stability analysis by including the lowest order quadratic nonlinearity in Eqs. (19) and (20). For this purpose we modify the ansatz (31) by allowing the constants a_0, b_0 to be slowly varying functions of time and transverse coordinate z :

$$\begin{pmatrix} A \\ B \end{pmatrix} = \begin{pmatrix} a_0(z, t) F_0'(x - x_0) \\ b_0(z, t) F_0(x - x_0) \end{pmatrix}. \quad (\text{B1})$$

We replace $\lambda \rightarrow \partial_t$ and $iq \rightarrow \partial_z$ in Eqs. (30) and add the corresponding quadratic nonlinearity. Following the lines of Sec. IV D, we employ the solvability conditions in Eqs. (19)

and (20) using the ansatz (B1). The solvability conditions give rise to the following equations:

$$\partial_t a_0 = \partial_z^2 a_0 + 4k \partial_z b_0 - 2a_0/u - d_1 a_0^2 + d_2 b_0^2, \quad (\text{B2})$$

$$\partial_t b_0 = \partial_z^2 b_0 - k \partial_z a_0 - d_3 a_0 b_0. \quad (\text{B3})$$

The constant $d_{1,2,3}$ are given by the integrals

$$\begin{aligned} d_1 &= \frac{3}{i_2} \int_{-\infty}^{\infty} F_0 (F_0')^3 e^x dx, \\ d_2 &= \frac{1}{i_2} \int_{-\infty}^{\infty} F_0^3 F_0' e^x dx, \\ d_3 &= \frac{2}{i_1} \int_{-\infty}^{\infty} F_0^3 F_0' e^x dx. \end{aligned} \quad (\text{B4})$$

Here we use Eqs. (34).

In general, we do not expect that Eqs. (B2) and (B3) have finite steady-state solutions in general case, because numerical simulations with Eq. (6) indicates that vortices tear off of the interface. The tearing off the vortices corresponds to a finite-time blow up of the solution of Eqs. (B2) and (B3).

However, there is a possibility that the solution remains finite very close to the threshold of the instability. In this case Eqs. (B2) and (B3) can be reduced to a single equation. In order to see that we perform the following transformation of variables:

$$\tilde{t} = \mu^4 t, \quad \tilde{z} = \mu z, \quad (\text{B5})$$

$$A = a_0 / \mu^4, \quad B = b_0 / \mu^3. \quad (\text{B6})$$

where $\mu^2 = 2uk^2 - 1$ is the supercriticality parameter characterizing the distance from the instability threshold. This particular scaling of the parameters will be clear later. After the transformation Eqs. (B2) and (B3) assume the form

$$\mu^4 \partial_{\tilde{t}} A = \mu^2 \partial_{\tilde{z}}^2 A + 4k \partial_{\tilde{z}} B - 2A/u - d_1 \mu^4 A^2 + \mu^2 B^2, \quad (\text{B7})$$

$$\mu^2 \partial_{\tilde{t}} B = \partial_{\tilde{z}}^2 B - k \partial_{\tilde{z}} A - \mu^2 d_3 A B. \quad (\text{B8})$$

We expand $A = A^{(0)} + \mu^2 A^{(1)} + \dots$ and $B = B^{(0)} + \mu^2 B^{(1)} + \dots$. In the lowest order in Eq. (B7) one obtains

$$A^{(0)} = 2uk \partial_{\tilde{z}} B^{(0)}. \quad (\text{B9})$$

In the next order one obtains

$$\begin{aligned} A^{(1)} &= 2uk \partial_{\tilde{z}} B^{(1)} + \frac{u}{2} \partial_{\tilde{z}}^2 A^{(0)} + \frac{ud_2}{2} (B^{(0)})^2 \\ &= 2uk \partial_{\tilde{z}} B^{(1)} + u^2 k \partial_{\tilde{z}}^3 B^{(0)} + \frac{ud_2}{2} (B^{(0)})^2. \end{aligned} \quad (\text{B10})$$

Thus combining Eqs. (B9) and (B10) one obtains the following relation between A and B :

$$A = 2uk\partial_z B + \mu^2 \left(u^2 k \partial_z^3 B + \frac{ud_2}{2} B^2 \right) + O(\mu^4). \quad (\text{B11})$$

Now, substituting A from Eq. (B11) into Eq. (B8) we obtain after simple algebra

$$\partial_t B = -\partial_z^2 B - k^2 u^2 \partial_z^4 B - ukB\partial_z B, \quad (\text{B12})$$

where $s = (2d_3 + d_2)$. This expansion is valid if $\mu^2 = 2uk^2 - 1 \rightarrow 0$, otherwise the reduction to a single equation is impossible. The coefficient s can be simplified by integration by parts:

$$\begin{aligned} s &= 2d_2 + d_2 = \left(\frac{2}{i_2} + \frac{2}{i_1} \right) \int_{-\infty}^{\infty} F_0^3 F_0' e^x dx \\ &= -\frac{5}{2i_1} \int_{-\infty}^{\infty} F_0^4 e^x dx \neq 0. \end{aligned} \quad (\text{B13})$$

Equation (B12) is the celebrated Kuramoto-Sivashinsky equation (KSE) known in the theory of pattern formation and interface growth models.^{19,20} In our situation KSE is valid only very close to the threshold of the instability. Simple comparison of omitted largest higher order nonlinear term $\sim d_1 \mu^2 u^3 k^3 \partial_z (\partial_z B)^2$ with the term $\sim ukB\partial_z B$ in Eq. (B12) gives the estimate $\mu^2 \ll 1/(u^2 k^2) \approx 1/u$.

-
- ¹T.W.B. Kibble, *J. Phys. A* **9**, 1387 (1976).
²W.H. Zurek, *Nature (London)* **317**, 505 (1985).
³N.D. Antunes, L.M.A. Bettencourt, and W.H. Zurek, *Phys. Rev. Lett.* **82**, 2824 (1999); J. Dziarmaga, P. Laguna, and W.H. Zurek, *ibid.* **82**, 4749 (1999); R.J. Rivers, *ibid.* **84**, 1248 (2000).
⁴T.W.B. Kibble and G.E. Volovik, *Pis'ma Zh. Éksp. Teor. Fiz.* **65**, 96 (1997) [*JETP Lett.* **65**, 102 (1997)].
⁵V.B. Eltsov, M. Krusius, and G.E. Volovik, cond-mat/9809125, in *Progress in Low Temperature Physics*, edited by W.P. Halperin, Vol. XV (North-Holland, in press).
⁶V.M.H. Ruutu, V.B. Eltsov, A.J. Gill, T.W.B. Kibble, Y.G. Makhlin, B. Placais, G.E. Volovik, and W. Xu, *Nature (London)* **382**, 334 (1996); V.M.H. Ruutu, V.B. Eltsov, M. Krusius, Y.G. Makhlin, B. Placais, and G.E. Volovik, *Phys. Rev. Lett.* **80**, 1465 (1998).
⁷V.B. Eltsov, T.W.B. Kibble, M. Krusius, V.M.H. Ruutu, and G.E. Volovik, *Phys. Rev. Lett.* **85**, 4739 (2000).
⁸N.B. Kopnin and E.V. Thuneberg, *Phys. Rev. Lett.* **83**, 116 (1999).
⁹I.S. Aranson, N.B. Kopnin, and V.M. Vinokur, *Phys. Rev. Lett.* **83**, 2600 (1999).
¹⁰L.P. Gor'kov and N.B. Kopnin, *Usp. Fiz. Nauk* **116**, 413 (1975) [*Sov. Phys. Usp.* **18**, 496 (1976)].
¹¹N.B. Kopnin, B.I. Ivlev, and V.A. Kalatsky, *J. Low Temp. Phys.* **90**, 1 (1993).
¹²A.T. Dorsey, *Phys. Rev. B* **46**, 8376 (1992).
¹³R.J. Donnelly, *Quantized Vortices in He-II* (Cambridge University Press, Cambridge, 1991).
¹⁴I.S. Aranson and V. Steinberg, *Phys. Rev. B* **54**, 13 072 (1996).
¹⁵P.C. Hohenberg and B.I. Halperin, *Rev. Mod. Phys.* **49**, 435 (1977).
¹⁶A.J. Leggett, *Rev. Mod. Phys.* **47**, 331 (1975).
¹⁷Even for $T_f = 0$ there is a small level of fluctuation due to round-off effects in numerical integration. For single precision it may generate noise with the strength $T_f \sim 10^{-6}$.
¹⁸L. M. Pismen, *Vortices in Nonlinear Fields* (Oxford University, New York, 1999), p. 114.
¹⁹Y. Kuramoto, *Chemical Oscillations, Waves and Turbulence* (Springer-Verlag, Berlin, 1984).
²⁰M.C. Cross and P.C. Hohenberg, *Rev. Mod. Phys.* **65**, 851 (1993).
²¹A.A. Nepomnyashchii, *Europhys. Lett.* **31**, 437 (1995).
²²H. Sakaguchi, *Prog. Theor. Phys.* **89**, 1123 (1993).
²³Equation (41) estimates the number of vortices created as a result of interface instability whereas Fig. 9 displays the outcome of the whole nucleation process, both in the bulk and the interface.
²⁴A. Yates and W.H. Zurek, *Phys. Rev. Lett.* **80**, 5477 (1998).
²⁵W.F. Vinen, *Proc. R. Soc. London, Ser. A* **242**, 493 (1957).
²⁶V.V. Ginzburg, L. Radzihovsky, and N.A. Clark, *Phys. Rev. E* **55**, 1 (1997).
²⁷I. Spolatorov and P. Krapivsky, *Phys. Rev. E* **53**, 3154 (1996).
²⁸P.J. Hakonen and V.P. Mineev, *J. Low Temp. Phys.* **67**, 313 (1987).
²⁹S. Ducci, P.L. Ramazza, W. González-Viñas, and F.T. Arecchi, *Phys. Rev. Lett.* **83**, 5210 (1999).